Effects of nonresonant hot ions with large orbits on Alfvén cascades and on magnetohydrodynamic instabilities in tokamaks

S. E. Sharapov
Euratom/UKAEA Fusion Association, Culham Science Centre, Abingdon, Oxfordshire OX14 3DB, United Kingdom

A. B. Mikhailovskii
Institute of Nuclear Fusion, RRC Kurchatov Institute, Kurchatov Sqr. 1, Moscow 123182, Russia and Moscow Institute of Physics and Technology, Dolgoprudnyi, Moscow Region, Russia

G. T. A. Huysmans
Association EURATOM-CEA Cadarache, 13108 St. Paul-Lez-Durance, France

(Received 16 October 2003; accepted 3 February 2004; published online 19 April 2004)

The effects of nonresonating hot ions on the spectrum of magnetohydrodynamic (MHD) waves and instabilities in tokamaks are studied in the limit when the width of the hot ion drift orbits is much larger than the radial scale length of the MHD perturbations. Due to the large magnetic drift velocities the hot ions cannot contribute to the MHD perturbations directly, but two main effects of the hot ions, the hot-ion density-dependent effect and the hot-ion pressure-dependent effect, influence the MHD perturbations indirectly. The physics of both effects is elucidated and it is shown that both these effects can be described in MHD approach. A new code, MISHKA-H (MISHKA including the hot-ion indirect effects), is developed as an extension of the ideal MHD code MISHKA-D [Huysmans *et al.*, Phys. Plasmas **8**, 4292 (2002)]. Analytical benchmarks for this code are given. Results of the MISHKA-H code on Alfvén spectrum in a shear-reversed discharges with ion-cyclotron resonance frequency (ICRF) heating are presented. Modeling of Alfvén cascades and their transition into toroidal Alfvén eigenmodes in shear-reversed tokamak equilibrium is considered. The hot-ion effect on the unstable branch of the MHD spectrum is studied for the test case of an $n=1$ ideal MHD internal kink mode, which is relevant to short-period sawteeth in low-density plasmas observed in Joint European Torus (JET) [Rebut *et al.*, *Proceedings of the 10th International Conference, Plasma Physics and Controlled Nuclear Fusion, London* (International Atomic Energy Agency, Vienna, 1985), Vol. I, p. 11] experiments with high-power ICRF heating.
 [DOI: 10.1063/1.1690303]

I. INTRODUCTION

A significant population of hot ions with large drift orbits is typical of present-day tokamak experiments in which high-power ion-cyclotron resonance frequency (ICRF) heating is applied in plasmas with low central current[1] or in low-density plasmas.[2] New magnetohydrodynamic (MHD) phenomena were revealed in such regimes, e.g., upward frequency-sweeping phenomena named Alfvén cascades (ACs) in discharges with nonmonotonic safety factor on Joint European Torus (JET)[3,4] and on JT-60U,[5] and short-period sawteeth on JET.[2]

Analytical study and numerical simulations of these phenomena are both required in assessing their physics. The first step in the analytical study has been made in Ref. 6, where the JET experiments exhibiting the ACs have been interpreted. It has been found in Ref. 6 in the drift kinetic approach that nonresonant hot ions with drift orbit width larger than the width of the MHD perturbation can nonperturbatively alter the structure of the Alfvén spectrum and give rise to a new type of Alfvén eigenmodes in a strong shear-reversed equilibrium. These modes are essentially associated with the minimum value of the safety factor $q_{\min}$ and they possess all the main properties of the experimentally observed Alfvén cascades.[3] An important peculiarity of the hot-ion effect studied in Ref. 6 is the dependence of this effect on the density gradient of hot ions. Therefore, this hot-ion effect can be called the *hot-ion density-dependent effect*. The main goal of the present work is the development of a MHD code for numerical simulations of the large-orbit hot-ion effects and employment of this code to JET-relevant problems. The other goals are the understanding of the physics of the phenomena considered and formulating analytical benchmarks for the numerical simulations.

In the code development, a modification of the existing MISHKA[7,8] code is performed. The MISHKA-type codes were designed to include not only the standard MHD effects, such as incorporated, e.g., in the CASTOR code,[10] but to accommodate a variety of effects described in Ref. 9. These effects are the finite ion Larmor radius effect and the electron and ion drift effects as well as the effects of neoclassical bootstrap current, neoclassical ion viscosity, and the collisionless skin effect. However, the effects of hot ions were out of the scope of this initial program on the MISHKA codes,[9] since a general approach to the hot ion effects requires MHD treatment of specifically kinetic effects such as the wave-particle resonant interaction. Such kinetic effects are essential, for instance, for the energetic particle modes (EPMs).[11–13] However, in the frame of the standpoint of Ref.

9 the incorporation of the resonant interaction effect in MHD codes is problematic.

In this connection, a question arises whether the hot-ion effect studied in Ref. 6 can be included into the MHD codes. The mechanism of the hot-ion density-dependent effect was not considered in Ref. 6 in the MHD approach in order to answer this question. Meanwhile, the notion of this effect was applied in Ref. 14 to the theory of magnetic islands, where it was explained that the effect considered is in fact caused by electrons compensating the equilibrium charge of the hot ions. Due to their cross-field motion in the electric field of perturbations, these compensating electrons lead to the drift (convective) contribution into the current continuity equation, thereby resulting in an electron term proportional to the density gradient of the hot ions.

Since an incorporation of the hot-ion density-dependent effect in the MISHKA-type codes means in fact an accomodation of additional terms governing the *electron* drift, the effect studied in Ref. 6 can be incorporated into the MISHKA codes. Evidently, this effect should be considered as an *indirect effect of hot ions*, in contrast to the *direct effects of hot ions*, the example of which has been considered in Refs. 11–13.

The mechanism of the hot-ion density-dependent effect is somewhat similar to that of the Varma–Shukla effect[15] studied in the theory of dusty plasma. In such plasma, charged dust particles have a very large mass and are not involved in perturbed dynamics, also revealing the cross-field effect of noncompensated electrons or ions.

In general, the hot-ion density-dependent effect can essentially alter both the stable and the unstable spectrum of MHD eigenmodes. Meanwhile, for some equilibria the consequences of this effect are more profound. In particular, in tokamak equilibria with a strongly reversed magnetic shear, the hot-ion density-dependent effect leads to the appearance of a new type of Alfvén eigenmode[6] which essentially differs from the toroidal Alfvén eigenmodes (TAEs). These new eigenmodes with eigenfrequencies outside the TAE-gap frequency and with a single dominant poloidal harmonics[6] are revealed in shear-reversal experiments as the Alfvén cascades.[3]

In addition to the density-dependent effect, an important pressure-dependent indirect effect of the large-orbit hot ions on MHD perturbations occurs naturally as the hot ions do contribute in equilibrium diamagnetic current but fail to contribute in the perturbed pressure of the MHD eigenmodes. It is known that for the MHD instabilities in the case of vanishingly small ion orbits, a mutual compensation occurs between the magnetic-well effect caused by the plasma diamagnetism and the perturbed parallel magnetic field effect caused by the perturbed plasma pressure [see, e.g., Ref. 16, Chap. 1 of Ref. 17, and Eq. (C.15) of Appendix C]. Since the large-orbit hot ions are not involved in the perturbed dynamics, they can not contribute into the last effect and, as a result, these ions lead to a noncompensated additional contribution into the magnetic well. This contribution is proportional to the pressure gradient of hot ions. Respectively, this indirect effect can be called the *hot-ion pressure-dependent effect*.

The magnetic-well effect is known to be important for MHD instabilities with characteristic mode growth rates and frequencies much smaller than those of the Alfvén modes (see, e.g., Chaps. 5–15 of Ref. 18 and references therein). Therefore, the hot-ion density-dependent effect is of interest, first of all, for the problem of the Alfvén modes, while the hot-ion pressure-dependent effect is of interest for the problem of MHD instabilities.

In physics terms, the hot-ion pressure-dependent effect is similar to the stabilizing effect of high energy ions on ballooning modes considered in Ref. 19. According to Ref. 19, this stabilizing effect can give limiting beta values exceeding the values predicted by the standard theory of ballooning modes (see Ref. 19 for details).

An important step in the theory of Alfvén eigenmodes in shear-reversal discharges has been made recently in Ref. 20. The subject of Ref. 20 is an analytic description of the hot-ion density-dependent effect and its competition with a toroidicity effect, which can cause a discrete Alfvén eigenmode associated with $q_{\min}$ in a weak shear reversal plasma. The essence of this paper is commented on in more detail below (see Sec. II).

Looking at the above-discussed hot-ion indirect effects with the standpoint of the program stated in Ref. 9, one can note that the pressure-dependent effect can be included in the MISHKA-type codes by redetermination of the equilibrium parameters. On the other hand, the density-dependent effect can be incorporated by adding an electron drift term similar to the ion drift terms allowed for in the MISHKA-D code.[8] Therefore, it is possible to include both these effects in the MHD approach used in the MISHKA codes. We have developed such a code and call it the MISHKA-H (MISHKA including the hot-ion indirect effects described above).

Section II is addressed to the physics treatment of the large-orbit hot-ion indirect effects. In Sec. III a description of the MISHKA-H model and its numerical method is given. Section IV yields analytical benchmarks for Alfvén eigenmodes. In Sec. V numerical results on these eigenmodes (computing the Alfvén cascades) are presented. Section VI demonstrates the pressure-dependent effect in the problem of the Bussac internal kink mode.[18,21] Conclusions are given in Sec. VII.

In addition, the paper contains Appendices A–F. In Appendix A, we collect equilibrium relations necessary for the physics treatment of the hot ion effects. In Appendix B, the equilibrium relations necessary for the code development are given. In Appendix C, we derive the perturbed current continuity equation, which is the basis for analysis performed in Sec. II. Appendix D addresses the derivation of a single-fluid momentum equation allowing for the hot-ion indirect effects. This equation is the basis for constructing the MISHKA-H model of Sec. III. Appendix E collects relations explaining the single-fluid description of the perturbed quantities that are necessary for the code. Appendix F is a mathematical supplement to the Introduction.

II. PHYSICS OF INDIRECT EFFECTS OF HOT IONS WITH LARGE ORBITS

A. Current continuity equation

Following a routine derivation (see Appendix C), we represent the current continuity equation to the problem in the form

$$\nabla_{\parallel}\tilde{j}_{\parallel}+\nabla_{\perp}\cdot\tilde{\mathbf{j}}^{I}+H_p+H_n=0. \tag{1}$$

Here $\tilde{j}_{\parallel}$ is the perturbed parallel current, $\tilde{\mathbf{j}}^{I}$ is the inertial current, and

$$H_p=\frac{c}{4\pi B_0^3}\mathbf{b}_0\cdot[\nabla\tilde{p}_c\times\nabla p_{0h}], \tag{2}$$

$$H_n=-e_h\mathbf{V}_E\cdot\nabla n_{0h}, \tag{3}$$

and the remaining definitions are given in Appendix C.

The terms H_p and H_n describe the two effects that depend on the pressure and density gradients of the hot ions, respectively. The density-dependent effect was studied in the kinetic approach in Ref. 6, while the pressure-dependent effect was studied in kinetic approach in Ref. 19.

B. Physics of pressure-dependent effect

In order to understand the physics of the effect represented by (2) let us turn to Appendix C. The first term in the brackets on the right-hand side of Eq. (C11) describes the magnetic well due to the diamagnetism of the core plasma. When the hot ions with large orbits are absent, the diamagnetic well is compensated by the effect of the perturbed parallel magnetic field $\tilde{B}_{\parallel}$. Then, one arrives at the well-known result (see, e.g., Ref. 16) that no magnetic well appears in the case of the equilibrium magnetic field with straight field lines. However, since the hot ions contribute in the diamagnetic effect and do not contribute into $\tilde{B}_{\parallel}$, this noncompensated effect of the hot ion diamagnetism causes a magnetic-well effect.

In order to determine the sign of the magnetic-well effect induced by hot ions, we consider the perturbations in the form $f(x)\exp(-i\omega t+ik_x x+ik_y y)$, where ω is the mode frequency, k_x and k_y are the respective projections of the wave vector, $f(x)$ is a slowly varying amplitude, and $|d\ln f/dx|\ll k_x$. For simplicity, we keep only the inertial term in Eq. (1) and the term with the magnetic well. In this case

$$\tilde{\mathbf{j}}^{I}=-i\frac{\omega\rho_0 c^2}{\mathbf{B}_0^2}\tilde{\mathbf{E}}, \tag{4}$$

so that Eq. (1) reduces to

$$\rho_0\omega(\mathbf{k}_{\perp}\cdot\tilde{\mathbf{E}})-i\frac{k_y\tilde{p}_c}{4\pi cB_0}\frac{dp_{0h}}{dx}=0. \tag{5}$$

Here, $\mathbf{k}_{\perp}=(k_x,k_y)$, $\rho_0=m_i n_{0i}$ is the equilibrium mass density, and m_i is the core ion mass. The main contribution in the perturbed plasma pressure $\tilde{p}_c$ is due to the cross-field convection, i.e., it is determined by the equation

$$\partial\tilde{p}_c/\partial t+\mathbf{V}_E\cdot\nabla p_{0c}=0, \tag{6}$$

so that

$$\tilde{p}_c=-i\frac{c\tilde{E}_y}{B_0\omega}\frac{\partial p_{0c}}{\partial x}. \tag{7}$$

In addition, we take

$$\tilde{\mathbf{E}}_{\perp}=-\nabla_{\perp}\tilde{\phi}, \tag{8}$$

where $\tilde{\phi}$ is the perturbed electrostatic potential. As a result, we obtain from Eq. (5) the local dispersion relation

$$\omega^2=\frac{1}{4\pi\rho_0 B_0^2}\frac{k_y^2}{k_{\perp}^2}\frac{dp_{0h}}{dx}\frac{dp_{0c}}{dx}. \tag{9}$$

One can see from Eq. (9) that if the hot ion pressure gradient is directed along the pressure gradient of the core ions,

$$\frac{dp_{0h}}{dx}\frac{dp_{0c}}{dx}>0, \tag{10}$$

the effect of the magnetic well is stabilizing, $\omega^2>0$. In the opposite case, i.e., for

$$\frac{dp_{0h}}{dx}\frac{dp_{0c}}{dx}<0, \tag{11}$$

this effect is destabilizing, i.e., one obtains a magnetic hill in this case.

In order to estimate when the hot-ion magnetic well becomes important, one can compare the estimate for the mode frequency Eq. (9) with the characteristic frequency of the flute instability in tokamaks (see, e.g., Sec. 9 of Ref. 22):

$$\omega^2\simeq\frac{k_y^2}{k_{\perp}^2}\frac{r_0}{\rho_0 R_0^2}\frac{dp_{0c}}{dx}. \tag{12}$$

Here r_0 is the radial coordinate labelling the magnetic surface at which the mode is localized, and R_0 is the major radius of the torus. Comparing Eqs. (9) and (12) we conclude that the hot ion effect on the magnetic well should be taken into account in addition to the standard magnetic well, if

$$\beta_h\geqslant r_0/(\kappa_n R_0^2). \tag{13}$$

This estimate was made for the flute-type modes with high poloidal m and toroidal n mode numbers, $(m,n)\gg 1$. In the case of the $m\cong n\cong 1$ kink mode (the Bussac mode) it should be modified (see Sec. VI).

C. Physics of density-dependent effect

One can see from Eq. (3) that the density-dependent effect is related to the cross-field motion of electrons that compensate the electric charge of the hot ions. Even though this charge is relatively small, the electron cross-field motion can be essentially stronger than the inertial motion of the core ions. Using Eqs. (4) and (8), we estimate

$$\nabla_{\perp}\tilde{\mathbf{j}}_{\perp}\cong\frac{\rho_0\omega c^2}{B_0^2}k_{\perp}^2\tilde{\phi}, \tag{14}$$

while, according to Eq. (3),

$$H_n \cong e_h \frac{\partial n_{0h}}{\partial x} \frac{ck_y}{B_0} \tilde{\phi}, \tag{15}$$

so that the density-dependent effect is comparable to the inertial effect for

$$\frac{\omega}{\omega_{Bi}} \cong \frac{e_h}{e_i} \frac{1}{n_{0c}} \frac{\partial n_{0h}}{\partial x} \frac{k_y}{k_\perp^2}, \tag{16}$$

where $\omega_{Bi}=e_iB_0/(m_ic)$ is the core ion cyclotron frequency. This condition holds for Alfvén eigenmodes studied in Ref. 6.

D. Relative role of pressure-dependent and density-dependent effects

Using Eqs. (2), (7), (8), and (15), we obtain

$$\left|\frac{H_p}{H_n}\right| \cong \beta_h \frac{n_{0i}}{n_{0h}} \cdot \frac{(1+\tau)\omega_{*pi}}{\omega}, \tag{17}$$

where

$$\omega_{*pi}=k_y(cT_{0i}/e_iB_0)d\ln p_{0i}/dx \tag{18}$$

is the diamagnetic drift frequency of core ions, and $\tau=T_{0e}/T_{0i}$ is the ratio of electron and core ion temperatures. It follows from Eq. (17) that high-frequency modes, $\omega \geqslant \omega_{*pi}$, similar to those studied in Ref. 6, are not affected by the effect of the hot ion pressure gradient. On the other hand, low-frequency modes, $\omega \cong \omega_{*pi}$, are significantly affected by the pressure gradient of the hot ions if

$$\beta_h \geqslant n_{0h}/n_{0i}. \tag{19}$$

Condition (19) implies that the hot ions are super-Alfvénic, $V_{Th} \geqslant V_A(m_h/m_i)^{1/2}$, where V_{Th} is the characteristic velocity of the hot ions.

E. Concept of "finite-frequency" magnetic well

Below we analyze the density-dependent effect on Alfvén eigenmodes representing the stable part of the MHD spectrum (waves), and the hot-ion pressure-dependent effect on the Bussac mode,[21] which is an example of the unstable MHD mode. It appears to be important to study both the Alfvén eigenmodes and the MHD instabilities under a simultaneous influence of the both hot-ion effects. The pressure-dependent effect on the Alfvén eigenmodes can be essential when the eigenfrequencies of these modes are not too high due to a small value of the effective parallel wave number $k_{\|\min}$. On the other hand, if one investigates not only the thresholds of MHD instabilities but their growth rates, γ, as well, then the density-dependent effect proportional to the mode frequency $\omega=i\gamma$ can be essential. A somewhat similar evaluation of "frequency-dependent" effects on MHD instabilities has been recently presented in Ref. 23 where the plasma compressibility effect on the growth rates of the instabilities was studied.

In the theory of MHD instabilities, all the effects causing an appearance of a discrete spectrum of unstable eigenmodes can be associated with a magnetic well of "zero-ω," since the eigenmodes considered at the threshold have vanishingly small frequencies. In this context, the frequency-dependent effects leading to the appearance of eigenmodes with finite ω in both the Alfvén cascade theory and in the theory of MHD instabilities can be called "ω-dependent magnetic well." The sum of both the "ω-dependent magnetic well" and the "zero-ω magnetic well" naturally lead us to a concept of a "finite-frequency magnetic well."

In the scope of such concept, it is important to delineate the parts of the "ω-dependent magnetic well" due to the hot ions and due to the core plasma. Calculations of both parts of the "ω-dependent magnetic well" were presented in Ref. 20. The results of Ref. 20 are described in Sec. IV D.

III. THE MISHKA-H MODEL

A. General comments on the MISHKA codes

The codes of the MISHKA series[7–9] are a continuation of the CASTOR code (see Ref. 10 and references therein). A key feature of the CASTOR code is to use the vector potential of the perturbed electromagnetic field. The main difference between the MISHKA series and the CASTOR code lies in the use of optimized variables characterizing the vector potential and the plasma velocity, and in an optimized form of linearized MHD equations. The optimized variables used in Ref. 7 are the "radial" (across the equilibrium magnetic surfaces) and the "parallel" (along the equilibrium magnetic field $\mathbf{B}_0$) projections of the vector potential $\mathbf{A}$ and the perturbed plasma velocity $\mathbf{V}$ and the radial components of the vector products of $\mathbf{A}$ and $\mathbf{V}$ with $\mathbf{B}_0$ called conventionally the "binormal" projections (see in detail Appendix E). The essence of the optimization of the MHD equations is the use of, first, the radial and parallel projections of the vector plasma motion equation as well as the vector product of this equation with the field $\mathbf{B}_0$, and, second, the similar projections of the vector Ohm's law. In making the choice of the optimized variables, and in optimizing the projections of the vector equations, one should also allow for the difference between the contravariant and covariant projections. Such optimization allows one, on the one hand, to eliminate the number of variables and equations in analyzing reduced problems, such as the ideal MHD modes[7] and their stabilization by the ω_{*i}-effect,[8] and, on the other hand, to augment the standard MHD equations by relatively simple terms describing the non-MHD effects.[9]

The CASTOR code[10] allows for resistivity and compressibility. It deals with seven variables: three components of plasma velocity, three components of the vector potential, and the perturbed plasma pressure. Formally, the CASTOR code includes the eighth variable as well, the perturbed plasma density, but the simultaneous considering of both the perturbed pressure and density is insignificant in practice if one neglects the thermal conductivity. In contrast to the CASTOR code, the MISHKA-1[7] is designed for the analysis of the ideal MHD modes in an incompressible plasma, and it solves a set of four equations for four variables: two components of the vector potential, both the radial and binormal projections. Such a simplification is a result of that, within the scope of this code, the parallel projection of the vector potential is excluded due to a vanishing parallel resistivity, the parallel plasma velocity is "thrown away" due to ne-

glecting the compressibility, while the perturbed plasma pressure is expressed in terms of the binormal projections of the vector potential. At the same time, in the development of the MISHKA-1 code, an additional simplifying circumstance has been used. The matter is that, due to the vanishing perpendicular resistivity, the velocity is algebraically expressed in terms of the vector-potential, being the product of this potential and the mode growth rate, and, in addition, the left-hand side of each projection of motion equation is the product of the velocity and the growth rate, while the right-hand side is a linear functional of the vector potential. Therefore, the four equations for four variables, each containing the first degree of the growth rate, are reduced to two equations for two variables (two velocity projections) containing the squared growth rate (see in detail Ref. 7).

The starting equations of the MISHKA-D code,[8] which allow for the ω_{*i}-effect, are similar to those of MISHKA-1. There are four equations for four variables: radial and binormal components of both the vector potential and the perturbed fluid velocity. However, the right-hand sides of the motion equation of MISHKA-D contain in contrast to MISHKA-1 both the vector potential and velocity, and the set of four equations cannot be reduced to two equations as in MISHKA-1. Therefore, studying the ω_{*i}-effect, MISHKA-D uses four equations for four variables.

B. MISHKA-H model

According to Appendix E, the MISHKA-H model is described by the four variables A_1, $\hat{A}_2$, $\tilde{V}^1$, and $\hat{V}^2$ interrelated by the equations

$$\lambda A_1 = \hat{V}^2, \tag{20}$$

$$\lambda \hat{A}_2 = -\tilde{V}^1, \tag{21}$$

$$L^1 = R^{1(0)} + R^{1(h)}, \tag{22}$$

$$L^2 = R^{2(0)} + R^{2(h)}. \tag{23}$$

Here

$$L^1 \equiv \lambda \rho_0 \left(g_{11}\tilde{V}^1 + \frac{g_{12}}{fq}\hat{V}^2 \right), \tag{24}$$

$$L^2 \equiv \lambda \rho_0 \left(g_{12}\tilde{V}^1 + \frac{g_{22}}{fq}\hat{V}^2 \right), \tag{25}$$

and

$$R^{1(0)} \equiv \frac{\hat{\alpha}_1}{4\pi} - \frac{F}{4\pi R^2}\frac{\partial}{\partial s}\left\{ G\left[\frac{\partial}{\partial s}(fq\hat{A}_2) - \frac{\partial A_1}{\partial \vartheta} \right] \right\} + \rho_0 \frac{c}{efq}\left[-g_{11}\frac{p_{0i}'}{n_0}\frac{\partial \tilde{V}^1}{\partial \vartheta} + g_{12}\frac{\partial}{\partial s}\left(\frac{\tilde{V}^1 p_{0i}'}{n_0} \right) \right], \tag{26}$$

$$R^{2(0)} \equiv \frac{\hat{\alpha}_2}{4\pi} - \frac{F}{4\pi R^2} G \frac{\partial}{\partial \vartheta}\left[\frac{\partial}{\partial s}(fq\hat{A}_2) - \frac{\partial A_1}{\partial \vartheta} \right] + \rho_0 \frac{c}{efq}\left[-g_{12}\frac{p_{0i}'}{n_0}\frac{\partial \tilde{V}^1}{\partial \vartheta} + g_{22}\frac{\partial}{\partial s}\left(\frac{\tilde{V}^1 p_{0i}'}{n_0} \right) \right]. \tag{27}$$

The values $\hat{\alpha}_1$ and $\hat{\alpha}_2$ are introduced as follows:

$$\hat{\alpha}_1 = \frac{4\pi}{c} J(j_0^2 \tilde{B}^3 - j_0^3 \tilde{B}^2) - \frac{F}{qR^2}\frac{\partial}{\partial s}[J(M\tilde{B}^1 + N\tilde{B}^2)] + \frac{F}{qR^2}\left(\frac{\partial}{\partial \vartheta} + q\frac{\partial}{\partial \phi} \right)[J(L\tilde{B}^1 + M\tilde{B}^2)], \tag{28}$$

$$\hat{\alpha}_2 = \frac{4\pi}{c} J j_0^3 \tilde{B}^1 + \frac{F}{R^2}\frac{\partial}{\partial \phi}[J(M\tilde{B}^1 + N\tilde{B}^2)]. \tag{29}$$

The coefficients L, M, N, and G are defined by

$$L = g_{11}/J, \quad M = g_{12}/J, \quad N = g_{22}/J, \quad G = g_{33}/J = F/fq, \tag{30}$$

where f, q, R, and F are given by Eqs. (B4)–(B6), and g_{ik} with $(i,k)=(1,2,3)$ are the metric tensor components.

The values $R^{1(h)}$ and $R^{2(h)}$ describing the hot-ion density-dependent effect are given by

$$R^{(1h)} = \frac{e_h}{c} n_h \hat{V}^2 + \frac{\partial}{\partial s}\left(\hat{A}_2 \frac{\partial p_{0h}}{\partial s} \right) + 4\pi \frac{R^2}{F^2}\frac{\partial p_{0c}}{\partial s}\frac{\partial p_{0h}}{\partial s}\hat{A}_2, \tag{31}$$

$$R^{2(h)} = -\frac{e_h}{c} n_h fq \tilde{V}^1 + \frac{\partial \hat{A}_2}{\partial \vartheta}\frac{\partial p_{0h}}{\partial s}. \tag{32}$$

The functions $\tilde{B}^1$, $\tilde{B}^2$, and $\tilde{B}^3$ in Eqs. (28) and (29) are the contravariant projections of the perturbed magnetic field $\tilde{\mathbf{B}}$. They are expressed in terms of A_1 and $\hat{A}_2$ by Eqs. (E5)–(E7) for $\hat{A}_3 = 0$.

C. Description of numerical method

We make Eq. (E11) dimensionless as follows:

$$\lambda \rho_0 \left\{ \tilde{\mathbf{V}} + \frac{\tau}{\mathbf{B}_0^2}\mathbf{B}_0 \times \nabla\left(\frac{\hat{A}_2 p_{0i}'}{n_0} \right) \right\} = -\nabla \tilde{p}_c + \mathbf{H} + \tau_H \rho_H [\tilde{\mathbf{V}} \times \mathbf{B}_0] + E_H \tilde{p}_c \nabla \rho_H, \tag{33}$$

by normalizing the space coordinate, the magnetic field, the density, the pressure, and the velocity:

$$R^* = \frac{R}{R_0}, \quad \mathbf{B}^* = \frac{\mathbf{B}}{B_0}, \quad \rho^* = \frac{\rho}{\rho_0}, \quad p^* = \frac{4\pi p}{B_0^2}, \quad \mathbf{V}^* = \frac{\mathbf{V}}{V_A}, \quad t^* = \frac{tV_A}{R_0}, \quad \rho_H = \frac{\rho_h}{\rho_0}, \tag{34}$$

where R_0, B_0, ρ_0, and V_A are the major radius, magnetic field, density, and Alfvén velocity at the position of the magnetic axis. The thermal ion drift effect is governed by the dimensionless parameter $\tau = V_A/(\omega_{Bi}R_0)$, while the hot-ion

density-dependent effect is governed by the dimensionless cyclotron frequency and energy of the hot ions:

$$\tau_H \equiv \omega_{Bh}\tau_A, \tag{35}$$

$$E_H \equiv T_h/(m_h V_A^2). \tag{36}$$

In the numerical scheme, the variables X_1, X_2, X_3, and X_4 are introduced instead of $\tilde{V}^1$, $\hat{V}^2$, A_1, and $\hat{A}_2$:

$$X_1 = fq\tilde{V}^1, \quad X_2 = i\hat{V}^2, \quad X_3 = iA_1, \quad X_4 = fq\hat{A}_2. \tag{37}$$

These four unknown functions are Fourier expanded in both the toroidal and poloidal angle; their structure in the radial coordinate s is described in Hermite finite elements $H(s)$, i.e., the same discretization as used in the CASTOR code[10] is employed:

$$X = e^{\lambda t}e^{in\phi}\sum_{m=-\infty}^{+\infty} e^{im\vartheta}\sum_{\nu=1}^{N}(X_m)_\nu H_\nu(s), \tag{38}$$

where X is any function from the four functions above. Following the approach described in Ref. 7, the weak form is constructed by multiplying Eqs. (22) and (23) by $(\tilde{V}^1)^*$ and $(\hat{V}^2)^*/(fq)$ correspondingly and integrating over the volume $d\tau = Jdsd\vartheta d\phi$, where the star denotes the complex conjugate. The resulting equations are then solved in their weak form.[10] Since the equilibrium does not depend on the toroidal angle, the ϕ-integration can be done trivially. The weak forms of Eqs. (22) and (23) are obtained then as follows:

$$\lambda N_1 = M_1 + M_1^h, \tag{39}$$

$$\lambda N_2 = M_2 + M_2^h. \tag{40}$$

Here, N_1, N_2, M_1, and M_2 are given in Refs. 7 and 8. The weak forms M_1^h and M_2^h describing the hot-ion effects are defined by

$$M_1^h = \int [X_1^* X_2 A^h(1,2) + X_1^* X_4 A^h(1,4) + X_1'^* X_4 A^h(1',4)]\, dsd\vartheta, \tag{41}$$

$$M_2^h = \int X_2^* X_1 A^h(2,1)\, dsd\vartheta. \tag{42}$$

The matrix elements corresponding to the hot-ion effects are

$$A^h(1,2) = A^h(2,1) = -i\tau_H\rho_H\frac{R^2}{F}, \tag{43}$$

$$A^h(1,4) = -\frac{E_H}{fq}\frac{d\rho_H}{ds}\frac{\partial}{\partial s}\left(\frac{R^2}{F}\right) + \frac{R^2E_H}{F^2fq}\frac{dp_{0c}}{ds}\frac{d\rho_H}{ds}, \tag{44}$$

$$A^h(1',4) = -\frac{R^2E_H}{fqF}\frac{d\rho_H}{ds}, \tag{45}$$

$$A^h(2,4) = -m\frac{d\rho_H}{ds}\frac{R^2E_H}{Ffq}. \tag{46}$$

In order to generate weak forms of Eqs. (20) and (21), we represent these equations in the form

$$\lambda X_3 = X_2, \tag{47}$$

$$\lambda X_4 = -X_1. \tag{48}$$

By multiplying Eqs. (43) and (44) by X_3^*, and X_4^*, respectively, and integrating the results over (s,ϑ,ϕ) we obtain

$$\lambda N_3 = M_3, \tag{49}$$

$$\lambda N_4 = M_4. \tag{50}$$

The expressions for N_3, N_4, M_3, and M_4 are given in Ref. 8. Let us correct a misprint in the expression for M_4 in Ref. 8: it should be written $A(4,1)=1$ instead of Eq. (A13e) of Ref. 8.

IV. ANALYTICAL BENCHMARKS FOR ALFVÉN EIGENMODES GOVERNED BY HOT-ION DENSITY-DEPENDENT EFFECT

A. Starting mode equation

Using Eq. (8), one reduces Eq. (3) for the density-dependent effect to

$$H_h = -\frac{e_h c}{\mathbf{B}_0^2}\mathbf{B}_0\cdot[\nabla\tilde{\phi}\times\nabla n_{0h}]. \tag{51}$$

In neglecting the pressure-dependent effect, H_h given by Eq. (51), Eq. (1) takes the form

$$\nabla_\parallel\tilde{j}_\parallel + \nabla_\perp\cdot\tilde{\mathbf{j}}^I - \frac{e_h c}{\mathbf{B}_0^2}\mathbf{B}_0\cdot[\nabla\tilde{\phi}\times\nabla n_{0h}] = 0. \tag{52}$$

In addition, we neglect the core ion drift effect. According to Eq. (C9), in this case the inertial current $\tilde{\mathbf{j}}^I$ is given by

$$\tilde{\mathbf{j}}^I = \frac{c\rho_0}{\mathbf{B}_0^2}\left[\mathbf{B}_0\times\frac{\partial\mathbf{V}}{\partial t}\right], \tag{53}$$

with $\mathbf{V}$ determined by the right-hand side of Eq. (C8).

We take the time-space dependence of $\tilde{\phi}$ in the form

$$\tilde{\phi}\sim\exp(-i\omega t + im\vartheta - in\varphi)\,\phi(r), \tag{54}$$

where m and n are the poloidal and toroidal mode numbers, respectively.

B. Large-aspect ratio tokamak

Using Eqs. (53) and (54), by the standard approach presented in Secs. 7.1 and 29.1 of Ref. 18, Eq. (52) reduces to (compare with Ref. 6)

$$\frac{\partial}{\partial r}\left[\left(\frac{\omega^2}{V_A^2}-k_\parallel^2\right)\frac{\partial\phi}{\partial r}\right] - \frac{m^2}{r^2}\left(\frac{\omega^2}{V_A^2}-k_\parallel^2\right)\phi + \frac{4\pi e_h\omega}{cB_0}\frac{m}{r}\frac{\partial n_{0h}}{\partial r}\phi = 0, \tag{55}$$

where $k_\parallel$ is the parallel wave vector given by

$$k_\parallel = \frac{1}{R_0}\left[\frac{m}{q(r)} - n\right]. \tag{56}$$

According to Refs. 1, 2, and 6, the problem of Alfvén cascades (ACs) is relevant when the q-profile has a minimum $q = q_{\min}$ at the point $r = r_0$, so that in the vicinity of this point

$$q(r)=q_{\min}+\frac{(r-r_0)^2}{2}q''_{\min}, \tag{57}$$

where $q''_{\min}\equiv(d^2q/dr^2)_{r=r_0}$ is positive, $q''_{\min}>0$. Allowing for Eq. (56), for such a q-profile, the function $k_\parallel^2$ is given by Eq. (6) of Ref. 6, i.e., by

$$k_\parallel^2(r)=k_{\parallel\,\min}^2\left(1-\frac{r_0^2q''_{\min}}{mR_0k_{\parallel\,\min}q_{\min}}x^2\right), \tag{58}$$

where

$$k_{\parallel\,\min}=\frac{1}{R_0}\left(\frac{m}{q_{\min}}-n\right), \tag{59}$$

$$x=m(r-r_0)/r_0. \tag{60}$$

Using Eq. (58), one has

$$\frac{\omega^2}{V_A^2}-k_\parallel^2=\frac{r_0^2k_{\parallel\,\min}}{mR_0}\frac{q''_{\min}}{q_{\min}^2}(x^2+S), \tag{61}$$

where

$$S=\frac{\omega^2-\omega_A^2}{\omega_A^2}\frac{mR_0q_{\min}^2k_{\parallel\,\min}}{r_0^2q''_{\min}}, \tag{62}$$

$$\omega_A=|k_{\parallel\,\min}|V_A. \tag{63}$$

Allowing for Eqs. (60) and (61), Eq. (55) reduces to

$$\frac{\partial}{\partial x}\left[(x^2+S)\frac{\partial\phi}{\partial x}\right]+(Q-S-x^2)\phi=0, \tag{64}$$

where

$$Q=\frac{4\pi e_hR_0q_{\min}^2\omega}{cB_0r_0q''_{\min}k_{\parallel\,\min}}\frac{\partial n_{0h}}{\partial r}. \tag{65}$$

The mode equation (64) is in correspondence with Eq. (7) of Ref. 6. The difference in the signs of Q given by Eq. (65) and by similar equation of Ref. 6 is explained by the (ϑ,φ)-dependence of $\tilde{\phi}$ in the form $\exp(im\vartheta-in\varphi)$ [see Eq. (54)], in contrast to $\exp(in\varphi-im\vartheta)$ taken in Ref. 6.

C. Analyzing the mode equation

We are interested in localized solutions of Eq. (64). Such solutions are possible only if

$$Q>0. \tag{66}$$

At the same time, in order to eliminate strong continuum damping, we consider the localized solutions to be acceptable only if

$$S>0. \tag{67}$$

Turning to Eq. (62) and allowing for Eq. (59), one can see that, for a positive m, $m>0$, the condition given by Eq. (67) is satisfied for

$$(\omega^2-\omega_A^2)(m-nq_{\min})>0. \tag{68}$$

Thus, the acceptable solutions are ''super-Alfvénic,''

$$\omega^2>\omega_A^2, \tag{69}$$

for

$$m>nq_{\min} \tag{70}$$

or

$$k_{\parallel\,\min}>0. \tag{71}$$

In the contrary case, when

$$m<nq_{\min} \tag{72}$$

or

$$k_{\parallel\,\min}<0, \tag{73}$$

the acceptable solutions are of ''sub-Alfvénic'' type,

$$\omega^2<\omega_A^2. \tag{74}$$

Turning to Eq. (65) and allowing for $\partial n_{0h}/\partial r<0$ in Eq. (66), one finds that the super-Alfvénic modes should have a negative frequency ω,

$$\omega<0, \tag{75}$$

while the frequency of the sub-Alfvénic modes should be positive,

$$\omega>0. \tag{76}$$

Thus, the numerical code should predict both the super-Alfvénic and the sub-Alfvénic eigenmodes. Both types of eigenmodes can be excited with an external antenna technique. However, modes which can be excited by high-energy ions with a monotonic density profile are selected by the sign of the diamagnetic drift frequency of the hot ions, ω_{*h},

$$\omega_{*h}\approx\frac{m}{r_0}\frac{V_{Th}^2}{\Omega_h}\frac{\partial\ln n_{0h}}{\partial r}, \tag{77}$$

where $\Omega_h\equiv e_hB_0/(m_hc)$ is cyclotron frequency of the hot ions, and m_h is the mass of the hot ion. A mode can be excited by the hot ions only if its frequency is of the same sign as that of the diamagnetic drift frequency, $\omega/\omega_{*h}>0$. Since, according to Eq. (77), the value of ω_{*h} is negative, we conclude that only the super-Alfvénic modes are relevant to the ACs.

The mode equation (64) has the same mathematical structure as that describing the Suydam modes of a finite growth rate considered in Sec. 5.1 of Ref. 18 and references given therein. Therefore, one can use the approach of Ref. 18 in analyzing Eq. (64).

The possibility of the existence of localized solutions of Eq. (64) is determined by behavior of the function ϕ in the most remote region of x where the terms with S are not important. For this region Eq. (64) reduces to

$$\frac{\partial}{\partial x}\left(x^2\frac{\partial\phi}{\partial x}\right)+(Q-x^2)\phi=0. \tag{78}$$

The condition for localized solutions is (see also Ref. 6)

$$Q>\tfrac{1}{4}. \tag{79}$$

Under the condition (79) the function ϕ is given by

$$\phi\sim x^{-1/2}K_{i\alpha}(x), \tag{80}$$

where $K_{i\alpha}$ is the Bessel function of second kind with an imaginary argument,

$$\alpha=(Q-1/4)^{1/2}. \tag{81}$$

Substituting Eq. (65) into Eq. (79) and using Eq. (63), one finds that the threshold density gradient of the hot ions, $|\partial n_{0h}/\partial r|_{crit}$, is given by

$$\frac{1}{n_0}\left|\frac{\partial n_{0h}}{\partial r}\right|_{\text{crit}}=\frac{1}{4}\frac{r_0}{R_0}\frac{q''_{\min}}{q^2_{\min}}\frac{e}{e_h}\frac{c}{\omega_{pi}}. \tag{82}$$

Here $\omega_{pi}=(4\pi e^2 n_{0i}/m_i)^{1/2}$ is the core ion plasma frequency.

For small deviations from the threshold value of the hot-ion density gradient, i.e., for

$$Q-\tfrac{1}{4}\ll 1, \tag{83}$$

the eigenvalue S can be found analytically in the following way. In addition to the remote region, one should solve Eq. (64) in a region of sufficiently small x neglecting the small terms with x^2 and S in the second bracket on the left-hand side. Then Eq. (64) reduces to

$$\frac{\partial}{\partial x}\left[(x^2+S)\frac{\partial\phi}{\partial x}\right]+Q\phi=0. \tag{84}$$

Solutions of Eq. (84) are presented in Appendix F. These solutions should be asymptotically matched with the solutions determined by Eq. (80). As a result of such matching, one obtains

$$S=x_A^2\exp\left[-\frac{2\pi}{(Q-1/4)^{1/2}}\right], \tag{85}$$

where

$$x_A=2^4\exp(-C+\pi/2)=43.2, \tag{86}$$

and $C\approx 0.577$ is the Euler constant. Substituting S from Eq. (62) into Eq. (85), one finds an explicit expression for the mode frequency

$$\frac{\omega^2-\omega_A^2}{\omega_A^2}=x_A^2\exp\left[-\frac{2\pi}{(Q-1/4)^{1/2}}\right]\frac{r_0^2 q''_{\min}}{mR_0 q^2_{\min}k_{\parallel\,\min}}. \tag{87}$$

According to Eq. (85), the eigenvalue S increases with increasing Q. However, for $Q\geqslant 1$ the above-presented approach to analyzing the mode equation (64) is invalid. Then one can follow an alternative approach valid for the limiting case $Q\gg 1$. In this case it is convenient, instead of ϕ, to use the function Φ given by[6]

$$\Phi=(S+x^2)^{1/2}\phi. \tag{88}$$

Then Eq. (64) is transformed to[6]

$$\frac{\partial^2\Phi}{\partial x^2}+f(x)\Phi=0, \tag{89}$$

where

$$f(x)=\frac{Q}{S+x^2}-\frac{S}{(S+x^2)^2}-1. \tag{90}$$

The function $f(x)$ has an extremum at the point $x=0$, and this function is given by the following equation in the vicinity of this point:

$$f(x)=\frac{Q-S}{S}-\frac{Q}{S^2}x^2. \tag{91}$$

Then Eq. (89) reduces to the equation for the linear oscillator,

$$\frac{\partial^2\Phi}{\partial x^2}+\left(\frac{Q-S}{S}-\frac{Q}{S^2}x^2\right)\Phi=0. \tag{92}$$

The solution to this equation is

$$\Phi\sim\exp(-w^2/2)H_l(w),\quad l=0,1,2,..., \tag{93}$$

where H_l are the Hermite polynomials, and

$$w=xQ^{1/4}/S^{1/2}. \tag{94}$$

The eigenvalues are given by[6]

$$S=Q-(1+2l)Q^{1/2}. \tag{95}$$

For not too large l, $l\ll Q^{1/2}/2$, Eq. (95) reduces approximately to

$$S\approx Q. \tag{96}$$

Turning to Eq. (64), one can see that this result corresponds to the local approximation for $r=r_0$.

It follows from Eqs. (96), (62), and (65) that in this case the frequency of the eigenmodes is defined by

$$\omega^2-\omega\omega_h-\omega_A^2=0, \tag{97}$$

where

$$\omega_h=\frac{m_h}{m_i}\Omega_h\frac{r_0}{m}\frac{1}{n_0}\frac{\partial n_{0h}}{\partial r}. \tag{98}$$

Equation (97) is similar to the local dispersion relation for the drift-Alfvén waves [see, e.g., Eq. (3.44) of Ref. 21], in which, instead of ω_h, one has ω_{*pi} given by Eq. (18). In order of magnitude

$$\frac{\omega_h}{\omega_{*pi}}\cong\frac{1}{k_y^2\rho_i^2}\frac{e_hL_c}{e_iL_h}\frac{n_{0h}}{n_{0c}}, \tag{99}$$

where ρ_i is the ion Larmor radius of core ions, and L_c and L_h are the characteristic scale lengths of the gradients of the core ion pressure and hot ions, respectively. It follows then that one can neglect the ω_{*pi}-effect if the hot ion density is high enough

$$\frac{n_{0h}}{n_{0c}}>k_y^2\rho_i^2\frac{e_iL_n}{e_hL_c}. \tag{100}$$

For smaller values of n_{0h}/n_{0c} the ω_{*pi}-effect should be included in the analysis presented above.

D. The role of core plasma toroidicity on Alfvén cascades

According to Ref. 20, the Alfvén cascade existence is determined by the potential well, Q_{eff}, which is the sum of the effect of the hot ions, Q_{hot}, and the toroidal geometry effect, Q_{tor}:

$$Q_{\text{eff}}=Q_{\text{hot}}+Q_{\text{tor}}. \tag{101}$$

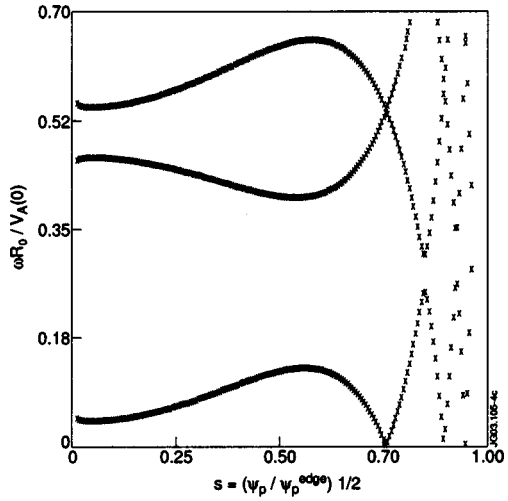

FIG. 1. Structure of the Alfvén continuum spectrum $|\omega_A(s)|$ for $n=3$ in the test case with nonmonotonic $q(r)$-profile, $q_{\min}=1.92$.

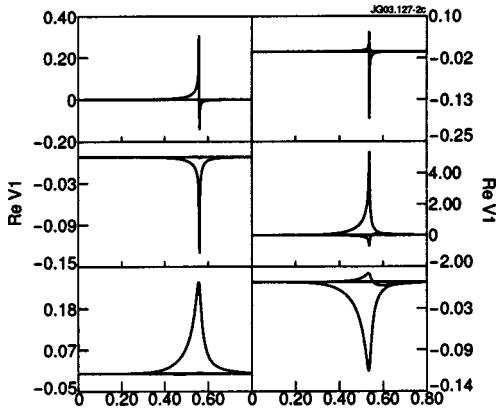

FIG. 2. MISHKA-H: computed eigenmodes of Alfvén Cascades associated with maximum of $|\omega_A(s)|$ (left, positive ω) and with minimum of $|\omega_A(s)|$ (right, negative ω), for $Q_{hot}=0.25$ (threshold), $Q_{hot}=0.4$ and $Q_{hot}=1$.

Here $Q_{\rm hot}$ is the same as the parameter Q given by Eq. (65) while the $Q_{\rm tor}$ is due to the core plasma alone determined by

$$Q_{\rm tor}=\frac{\omega^2}{2}\,\frac{R_0^2}{V_A^2(1-nq_{\min}/m)}\,\frac{q_{\min}^3}{r_0^2 q''_{\min}}\,\frac{\varepsilon_0(\varepsilon_0+2\Delta')}{1/4-(m-nq_{\min})^2}, \tag{102}$$

where $\varepsilon_0=r_0/R_0$ and Δ_0 is the Shafranov shift.

For not too high plasma pressure and small shear one can estimate $\Delta_0'=\varepsilon_0/4$ [see, e.g., Eq. (2.52) of Ref. 18]. Then one obtains

$$\frac{Q_{\rm hot}}{Q_{\rm tor}}=\frac{4}{3}\,\frac{r_0}{L_h}\,\frac{n_{0h}}{n_{0c}}\,\frac{\Omega_h}{\omega}\,\frac{1}{m\varepsilon_0^2}\,\frac{m_h}{m_i}\left[\frac{1}{4}-(m-nq_{\min})^2\right]. \tag{103}$$

For typical JET experimental parameters, $\Omega_h/\omega\cong 10^3$, $\varepsilon_0\cong 10^{-1}$, $m=nq_{\min}$, $n=3$, $r_0/L_h\cong 1$, and $n_{0h}/n_{0c}\cong 10^{-3}$, we arrive at the estimate

$$\frac{Q_{\rm hot}}{Q_{\rm tor}}\cong 20\cdot\frac{1}{q_{\min}}\left[\frac{1}{4}-(m-nq_{\min})^2\right]. \tag{104}$$

This estimate shows that in typical experimental conditions with high-power ICRF-heating the core plasma contribution into $Q_{\rm eff}$ is small. However, it is important to note that the toroidicity effect alone can also cause Alfvén cascade eigenmode in equilibrium with weakly reversed shear (for a small q'' value).

V. COMPUTING ALFVÉN CASCADES WITH THE MISHKA-H CODE

A. Alfvén cascades in the presence of hot-ions

We test the hot-ion effect on Alfvén cascades in a low-shear large-aspect ratio, $a/R_0=0.1$, equilibrium first. In such equilibrium, the potential well due to the toroidicity Q_{tor} is very small as compared to the well determined by the hot ion density gradient, $Q_{\rm hot}$, for a moderate hot ion pressure. Therefore, the general condition of the mode existence given by Eq. (79) reduces to $Q=Q_{\rm tor}+Q_{\rm hot}\approx Q_{\rm hot}>\frac{1}{4}$, and it is determined by the hot ion density gradient alone, with $Q_{\rm hot}$ given by Eq. (65).

Figure 1 shows the $n=3$ Alfvén continuum for the equilibrium used in this test case, with $q_{\min}\approx 1.92$, $d^2q/ds^2(r=r_{\min})\approx 1.105$, $r_{\min}/R_0\approx 0.0523$, and $\Delta'(r=r_{\min})\approx 0.013$. The MISHKA-H code was used then for a spectral analysis and a discrete eigenmode, the Alfvén cascade with $n=3$, $m=6$, was found to exist with an eigenfrequency above the Alfvén continuum with mode structure as shown in Fig. 2. By varying $n_{\rm hot}$ it was found that the eigenmode exists only at $n_{\rm hot}>n_{\rm hot}^{\rm crit}\approx 2.5\times 10^{-3}$, with the eigenmode width shrinking at the threshold as shown in Fig. 2. The corresponding values of $Q_{\rm hot}$ are given in the caption of Fig. 2, where the threshold value found is in agreement with the analytical estimate $Q_{\rm hot}=0.25$.

In order to investigate the transition from Alfvén cascades to toroidal Alfvén eigenmodes, a family of equilibria with the same profile of the current density, but with different $q_{\min}$, was generated. Figure 3 shows the computed evolution of two branches of the ACs, one with positive and the other with negative frequency, during a $q_{\min}$ decrease from 1.92 to 1.82. Formation of TAEs consisting of two dominant harmonics is observed similar to Ref. 20. Evolution of the corresponding frequencies of the eigenmodes in Fig. 3 is shown in Fig. 4 (cf. Ref. 20).

B. Alfvén cascades in a low-shear finite-aspect ratio tokamak

In a finite-aspect ratio tokamak, $a/R_0=0.3$, the potential well due to the toroidicity $Q_{\rm tor}$ can cause the existence of an AC eigenmode even without the hot ion density gradient, $Q_{\rm hot}=0$, provided the value of $q''_{\min}$ is small enough to satisfy Eq. (79). In order to test the condition of the Alfvén cascade existence due to the toroidicity effect alone, we assume the hot ion density to be zero and consider the condition [cf. (79)]

$$Q_{\rm eff}=Q_{\rm tor}+Q_{\rm hot}=Q_{\rm tor}>\tfrac{1}{4}, \tag{105}$$

determined by toroidicity effect alone.

A low-shear finite-aspect ratio equilibrium with $q_{\min}\approx 1.89$, $d^2q/ds^2(r=r_{\min})\approx 0.47$, $r_{\min}/R_0\approx 0.1$, and $\Delta'(r=r_{\min})\approx 0.044$ was tested with the MISHKA-H code for

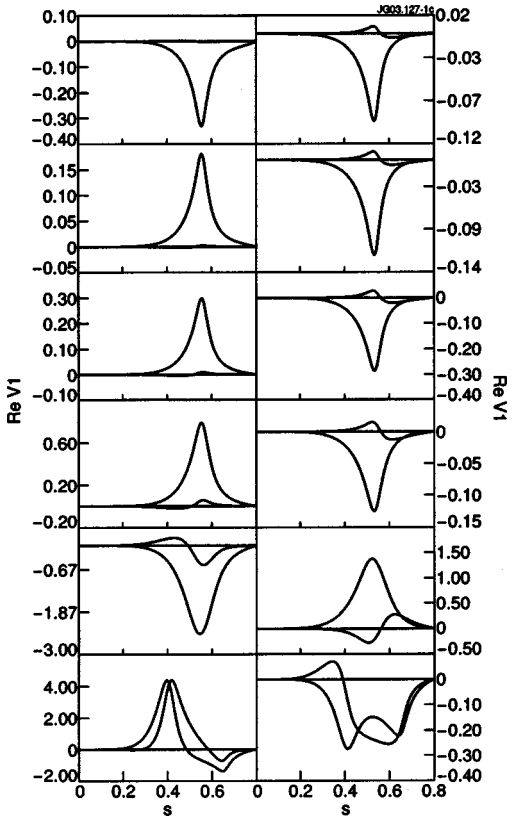

FIG. 3. MISHKA-H: evolution of Alfvén cascades associated with maximum of $|\omega_A(s)|$ (left, positive ω) and with minimum of $|\omega_A(s)|$ (right, negative ω), at $q_{\min}$ decreasing from 1.92 to 1.82. $Q_{hot}=0.7$.

$Q_{\rm hot}=0$. For the equilibrium parameters above, the value of $Q_{\rm tor}$ exceeds the threshold, $Q_{\rm tor}\approx 0.4>0.25$. The Alfvén continuum structure as a function of minor radius is shown in Fig. 5. For $Q_{\rm hot}=0$, we transit in fact to a version of the MISHKA-D code[8] with the ω_{*i}-effect neglected. An Alfvén cascade associated with $q_{\min}$ can be easily found in such equilibrium, with an example $n=1$, $m=2$ AC shown in Fig. 6.

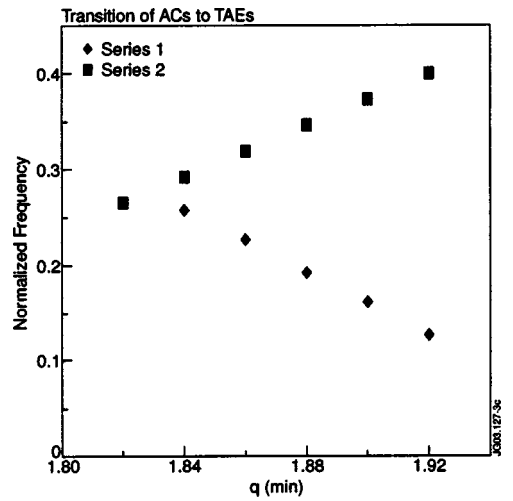

FIG. 4. MISHKA-H: evolution of normalized frequency, $|\omega R_0/V_{A0}|$, of Alfvén cascades shown in Fig. 3 at $q_{\min}$ decreasing from 1.92 to 1.82.

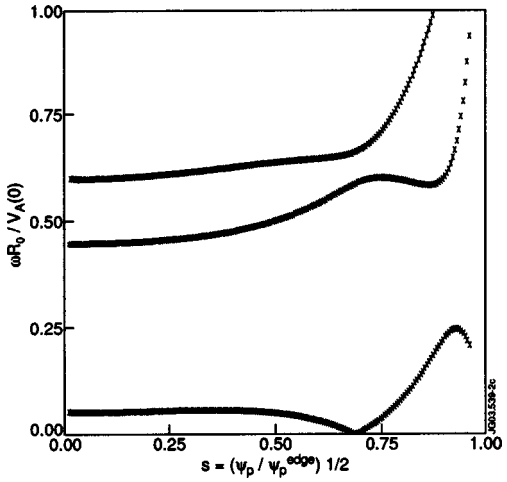

FIG. 5. Structure of the Alfvén continuum spectrum $|\omega_A(s)|$ for $n=1$ in the test case with nonmonotonic $q(r)$-profile and $Q_{tor}\approx 0.4$. $q_{\min}=1.89$.

C. Alfvén cascades in current hole discharges

Equilibria with zero density of the toroidal current in the near-axis plasma region are typical for the JET low-inductive current discharges with internal transport barriers. Alfvén cascades in such plasmas are almost always seen clearly in such discharges and they allow diagnostics of the evolution of $q_{\min}$ in such plasmas. Figure 7 shows plasma equilibrium with the current hole reconstructed with the motional Stark effect measurements in a typical JET discharge of this type, with $q(0)\geqslant 35$ and $q_{\min}\approx 1.8$. Figure 8 shows the structure of the Alfvén continuum computed with the CSCAS code for such equilibrium.

The MISHKA-H code was applied then and an Alfvén cascade with $n=2$ was obtained shown in Fig. 9. In contrast to the low-shear equilibrium described above, the AC mode does not consist of a single poloidal harmonic anymore, but it is strongly coupled to higher harmonics close to the current hole region.

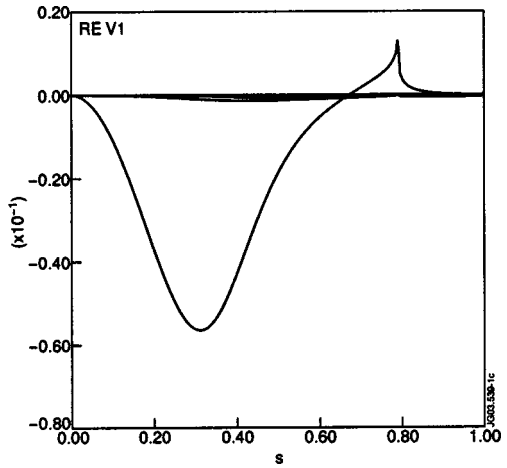

FIG. 6. Structure of the $n=1/m=2$ Alfvén cascade for the Alfvén continuum spectrum shown in Fig. 5.

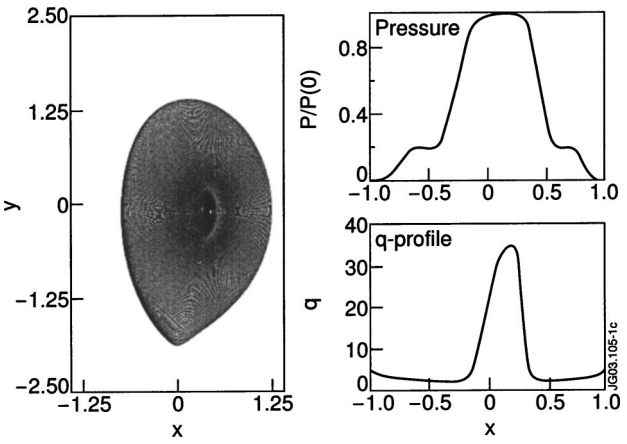

FIG. 7. Reconstructed equilibrium for JET current-hole discharge (pulse 55604) together with the total plasma pressure profile and the safety factor profile; $q_{\min}=1.8$, $q(0)=35$.

VI. ANALYTICAL BENCHMARKS AND NUMERICAL RESULTS ON THE PRESSURE-DEPENDENT EFFECT

A. Analytical benchmarks

By analogy with Sec. 5.1 and 13.3 of Ref. 18, using Eq. (C10), one can show that in allowing for the hot-ion pressure-dependent effect the growth rate of the Bussac mode is given by

$$\lambda=\lambda_H. \tag{106}$$

Here λ is the mode dimensionless growth rate and the parameter λ_H is equal to

$$\lambda_H=\lambda_H^{(c)}+\lambda_H^{(h)}, \tag{107}$$

where

$$\lambda_H^{(c)}=\kappa_B\frac{r_0^2}{R_0^2}\hat{S}(r_0)\left(3\beta_p^2-\frac{13}{48}\right), \tag{108}$$

$$\lambda_H^{(h)}=-\kappa_B\frac{4\pi}{B_0^2}\int_0^{r_0} r\frac{\partial p_{0c}}{\partial r}\frac{\partial p_{0h}}{\partial r}dr, \tag{109}$$

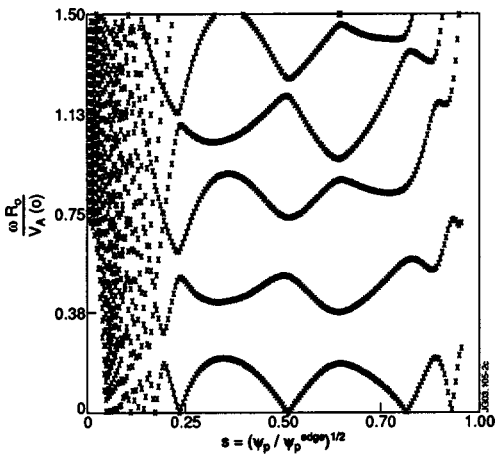

FIG. 8. Structure of the Alfvén continuum spectrum for JET current-hole discharge (pulse 55604).

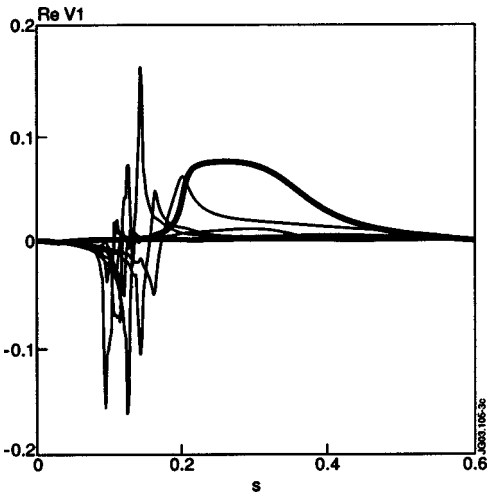

FIG. 9. Radial structure of the poloidal harmonics of the radial displacement of the $n=2$ Alfvén cascade eigenmode computed by the MISHKA-H code for JET current-hole discharge (pulse 55604). The eigenfrequency of this mode is $\omega R_0/V_A(0)=0.2289$, and the dominant poloidal harmonic, $m=4$, is plotted in solid line.

$$\kappa_B=\frac{\pi}{\hat{S}^2(r_0)B_\vartheta^2(r_0)}, \tag{110}$$

where $\hat{S}$ is the magnetic shear and r_0 is the mode resonant point satisfying the condition $q(r_0)=1$. It is assumed that in the region $r<r_0$ the magnetic shear is small and the core plasma pressure and the toroidal plasma current have parabolic radial distributions.

B. Numerical results

In order to assess the effect of hot ions on the unstable part of MHD spectrum, the MISHKA-H code is applied for calculating the stability limit of the internal kink mode.[21] A toroidal equilibrium with circular cross-section and $\varepsilon=0.10$ is analyzed. The pressure profile is chosen of the form

$$p=p_0(1-\overline{\psi}), \tag{111}$$

and the flux surface averaged current density

$$\langle j\rangle=j_0(1-\overline{\psi}), \tag{112}$$

where $\overline{\psi}=\psi/\psi_{edge}$ is the normalized poloidal flux. The kink mode was computed up to a hot ion pressure comparable to the thermal plasma pressure. The eigenmode structure consists of the principal $m=1$ poloidal harmonic and two satellites $m=0$ and $m=2$ as shown in Fig. 10. In Fig. 11 the growth rates of the kink mode are displayed as functions of the hot ion pressure for the hot ion pressure profile

$$p_{0h}=p_{0h}(1\pm 0.1\overline{\psi}), \tag{113}$$

for different values of the square of $\beta_p\equiv\beta_p(\psi_1)$, where $\beta_p(\psi_1)$ is defined as follows (compare with Refs. 18 and 21):

$$\beta_p=2\frac{(\int p(\psi)\,dA)/(\int dA)-p(\psi_1)}{B_p^2(\psi_1)}, \tag{114}$$

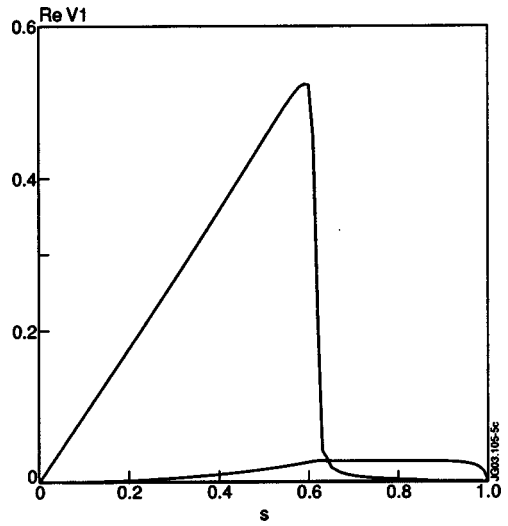

FIG. 10. Eigenmode of the Bussac internal $n=1$ kink in the presence of large orbit hot ions with $\beta_{\text{hot}}=\beta_{\text{thermal}}$.

where $dA=Jdsd\vartheta$, $\psi=\psi_1$ is the flux where $q(\psi)=1$ and $B_p(\psi_1)$ is the flux averaged poloidal magnetic field. As shown in Fig. 11, the linear dependence of λ on β_p^2 allows extrapolation to the marginal stability $\lambda=0$, but the value of the critical $(\beta_p^2)_{\text{crit}}$ depends on the hot ion pressure. For the hot ion profile given by Eq. (113), we obtain a reduction in the growth rates and the corresponding increase in $(\beta_p^2)_{\text{crit}}$. For an inverted hot ion profile, which could occur in experiments with off-axis ICRF-heating, i.e., for

$$p_{0h}=p_{0h}(1+0.1\overline{\psi}), \tag{115}$$

the hot ion effect becomes destabilizing as shown in Fig. 11.

VII. CONCLUSIONS

One can see that the analytical and numerical approaches to describing the linear MHD spectrum in this article meet at a ''cross-road'' of several trends in fusion-oriented plasma physics. First, we deal with the extended or ''generalized'' MHD which includes, in addition to the effects described by the standard single-fluid MHD, the core-ion drift effect (the ω_{*i}-effect) and the indirect density-dependent and pressure-dependent effects of hot ions. Second, our term ''*spectrum*'' implies all the varieties of *eigenmodes* including Alfvén eigenmodes representing the stable part of the spectrum, and numerous MHD instabilities in the unstable part of the MHD spectrum. Analytical and numerical approaches are coupled with each other, so that the analytical results are used as benchmarks for performing the numerical simulations, while the numerical simulations revealing some unexpected details of a physics phenomenon help to further development of a more perfected analytical approach to analyzing this phenomenon.

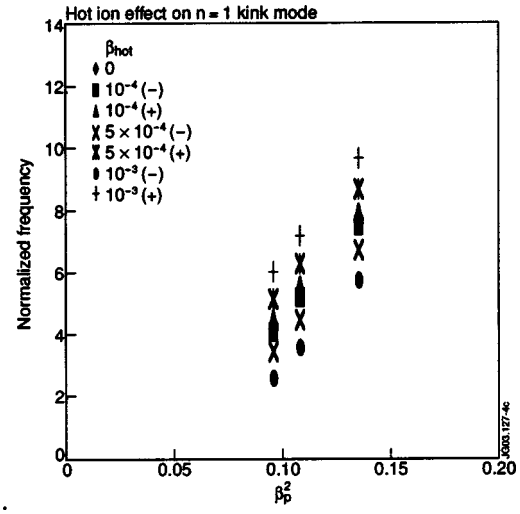

FIG. 11. Growth rates of the Bussac mode as functions of β_p^2, in the presence of large orbit hot ions with profiles $p_{\text{hot}}(0)(1-0.1\psi)$ [marked with $(-)$] and $p_{\text{hot}}(0)(1+0.1\psi)$ [marked with $(+)$].

In the scope of this article we have limited our studies by two specified cases only: the Alfvén cascades, and the Bussac internal $n=1$ kink mode.

It was explained in the Introduction that the Alfvén cascades have an important role in the JET experiments on internal transport barriers in reversed-shear equilibrium. Though initially the generation of Alfvén waves by hot ions was perceived as a harmful phenomenon leading to a worsening of the hot ion energy transfer to the core plasma, this type of phenomena recently attracted attention as plasma diagnostics. In particular, the Alfvén cascades became an important tool for the MHD spectroscopy of the reversed-shear discharges.[1,3,4] In the scope of the MHD spectroscopy based on the Alfvén cascades, the determination of the temporal evolution of $q_{\min}(t)$ from the clustering of different toroidal mode number ACs in time was performed.[1,4] Moreover, a close correlation between the integer $q_{\min}$ values, the so-called ITB triggering events, and the Alfvén grand-cascades (when ACs of all n's are excited simultaneously) was experimentally established on JET[3] and is widely used for obtaining ITBs in shear-reversed discharges.

Preceding numerical simulations of the Alfvén cascades made with the CASTOR,[24] NOVA,[25] and TASK/WM[26] codes were performed neglecting the hot-ion contribution into the Alfvén spectrum. In terms of the parameter Q_{eff} given by Eq. (101) this means that the term Q_{hot} given by Eq. (65) was neglected compared with the term Q_{tor} given by Eq. (102). This relation is valid for the case of alpha-particles in Ref. 25, but not for experimental conditions with ICRH-accelerated hot ions, where the opposite relation holds [see the estimate given by Eq. (104)]. Though the modes were found to exist in Refs. 24–26, these were due to the weakly nonmonotonic $q(r)$-profiles considered in these papers. However, for a broader family of equilibria with larger values of negative magnetic shear, the hot ion contribution is crucial for the mode formation as the cross-field motion of electrons compensating the equilibrium charge of the hot ions, the Q_{hot} term, is essentially stronger than the core plasma inertia leading to the Q_{tor} term (see in detail Sec. II).

The Bussac mode, the $n=1$ internal kink mode, has been long recognized as a linear trigger for sawtooth oscillations.[27] The new type of short-period sawteeth, which were observed in JET low-density discharges[2] with high-power ICRF heating and with $\beta_{\text{hot}}\cong\beta_{\text{core}}$, could not be in-

terpreted in a perturbative approach with small orbit width.[28] The accomodation of the indirect pressure-dependent effect in the MISHKA-H code seems to be a relevant approach for understanding the physics of the short-period sawteeth in the future.

The MISHKA-H code was tested as follows. The threshold character of the appearance of the computed Alfvén cascades shown in Fig. 3 is in correspondence with the benchmark given by Eqs. (65) and (79). The results of numerical simulations of the Bussac mode presented in Figs. 9 and 10 are in agreement with the benchmarks given by Eqs. (106)–(110).

A part of our numerical simulations has been performed in neglecting the hot-ion effects corresponding to the scope of the MISHKA-D code[8] (see Figs. 4 and 5). These simulations, on the one hand, support the analytic theory of the Alfvén cascades caused by the toroidicity effect due to the core plasma alone,[20] and, on the other hand, can be considered as an additional test for the code developed.

For the real JET discharges with low inductive current and with internal transport barrier, the equilibrium with zero-density toroidal current in the central plasma region recently became important.[29] Computing the current hole equilibrium and studying both the Alfvén continuum and the Alfvén cascades in such equilibrium require a high level of accuracy and consistency between the equilibrium and MHD-spectrum codes involved. The capability of the MISHKA-H code to handle this type of equilibrium and to compute the Alfvén cascades observed experimentally was demonstrated in Figs. 7 and 9.

In summary, the MISHKA-H code seems to be an effective numerical tool for a routine analysis of the MHD spectrum in tokamak discharges with large-orbit hot ions generated at the ICRF heating of plasma. This code could be also generalized to the case of finite-orbit hot ions most relevant to the fusion discharges with α-particles.

ACKNOWLEDGMENTS

H. L. Berk, B. N. Breizman and S. D. Pinches are gratefully acknowledged for their comments and criticism during the MISHKA-H tests. The authors also like to thank J. G. Cordey for support and S. V. Konovalov and V. S. Tsypin for useful discussions.

This work was funded jointly by the United Kingdom Engineering and Physical Sciences Research Council and by EURATOM. One of the authors (A.B.M.) was also supported by the Russian Foundation for Basic Research, Grant No. 03.02.16294, by the Russian Federal Program on Support of Leading Scientific School Researches, Grant No. 2024.2003.2, by Department of Atomic Science and Technology of the Russian Ministry of Atomic Industry, and by US Civilian Research and Development Foundation for the Independent States of the Former Soviet Union, Grant No. BRHE REC-011. This work was performed in part under the European Fusion Development Agreement.

APPENDIX A: EQUILIBRIUM RELATIONS FOR THE PHYSICS TREATMENT OF THE INDIRECT EFFECTS OF THE HOT IONS

The equilibrium pressure of the core (thermal) plasma and of the hot ions is assumed to be isotropic and described by scalar functions p_{0c} and p_{0h}, which only depend on a radial coordinate labeling the equilibrium magnetic flux surfaces. Evidently, such an assumption is a model for the hot ions.

Both the thermal plasma and the hot ions contribute to equilibrium plasma pressure p_0 and the equilibrium electric current density $\mathbf{j}_0$ as follows:

$$p_0 = p_{0c} + p_{0h}, \tag{A1}$$

$$\mathbf{j}_0 = \mathbf{j}_{0c} + \mathbf{j}_{0h}, \tag{A2}$$

where $\mathbf{j}_{0c}$ and $\mathbf{j}_{0h}$ are currents of the core plasma and of the hot ions, correspondingly. We assume for simplicity that the current of the hot ions $\mathbf{j}_{0h}$ has only a component perpendicular to the equilibrium magnetic field $\mathbf{B}_0$, so that $\mathbf{j}_{0h}$ and p_{0h} are related through

$$\mathbf{j}_{0h} = \frac{c}{\mathbf{B}_0^2}[\mathbf{B}_0 \times \nabla p_{0h}]. \tag{A3}$$

Taking the equilibrium current in the form of Eq. (A2), we thereby take into account the hot ion contribution into the inhomogeneity of the equilibrium magnetic field since

$$\nabla \times \mathbf{B}_0 = \frac{4\pi}{c}(\mathbf{j}_{0c} + \mathbf{j}_{0h}). \tag{A4}$$

According to the equilibrium equation,

$$0 = -\nabla p_0 + \frac{1}{c}[\mathbf{j}_0 \times \mathbf{B}_0], \tag{A5}$$

and Eq. (A3), the part of the perpendicular thermal plasma current $\mathbf{j}_{0c\perp}$ is given by

$$\mathbf{j}_{0c\perp} = \frac{c}{\mathbf{B}_0^2}[\mathbf{B}_0 \times \nabla p_{0c}]. \tag{A6}$$

It follows from Eqs. (A3), (A4), and (A6) that for the simplest case of a slab geometry with $\mathbf{B}_0$ directed along the z-axis and the equilibrium gradients directed along the x-axis of the Cartesian coordinate system (x,y,z), the plasma pressure balance leads to

$$\kappa_B = -\tfrac{1}{2}(\beta_c \kappa_{pc} + \beta_h \kappa_{ph}). \tag{A7}$$

Here $\kappa_B \equiv d \ln B_0/dx$, $\kappa_{pc} \equiv d \ln p_{0c}/dx$, and $\kappa_{ph} \equiv d \ln p_{0h}/dx$ are the inverse characteristic scales of the inhomogeneity of equilibrium magnetic field, core plasma pressure, and hot ion pressure, respectively, and $\beta_c = 8\pi p_{0c}/B_0^2$ and $\beta_h = 8\pi p_{0h}/B_0^2$. The dependence of κ_B on κ_{ph} is an essential point of the present paper.

The equilibrium number density of the hot ions, n_{0h}, is assumed to be much smaller than that of the core ions, n_{0i}, so that the ratio n_{0h}/n_{0i} is small. At first sight, one could neglect this small parameter. However, as shown in Sec. II, under certain conditions the small ratio n_{0h}/n_{0i} is amplified by a large ratio between the cross-field effect related to

plasma perturbations and the perpendicular inertia effect, so that the resulting effect of n_{0h}/n_{0i} can be essential. Therefore, we take the quasineutrality condition allowing for n_{0h}:

$$e_e n_{0e} + e_i n_{0i} + e_h n_{0h} = 0, \tag{A8}$$

where e_e, e_i, and e_h are the electric charges of the core plasma electrons, thermal ions, and hot ions, respectively, and n_{0e} is the equilibrium number density of electrons.

APPENDIX B: EQUILIBRIUM RELATIONS USED IN THE MISHKA-H CODE

We use the coordinate system s, ϑ, ϕ related to the magnetic surfaces with straight magnetic field lines similar to Ref. 7:

$$B_0^1 = 0, \tag{B1}$$

$$B_0^3/B_0^2 = q(s), \tag{B2}$$

where $s=(\psi/\psi_{\text{edge}})^{1/2}$ is the radial coordinate marking the magnetic surfaces, ϑ is the poloidal coordinate, ϕ is the toroidal angle, B_0^i $[i=(1,2,3)]$ are the contravariant components of the equilibrium magnetic field $\mathbf{B}_0$, and q is the safety factor. This coordinate system is specified by representing the magnetic field in the form

$$\mathbf{B}_0 = \nabla\phi \times \nabla\psi + F\nabla\phi, \tag{B3}$$

where $\psi=\psi(s)$ and $F=F(s)$ are the functions characterizing the poloidal and toroidal magnetic fluxes, correspondingly. According to Eq. (B3),

$$B_{03} = F, \tag{B4}$$

$$B_0^2 = f/J, \tag{B5}$$

where B_{03} is the ϕ-covariant component of $\mathbf{B}_0$, $f \equiv d\psi/ds$, and J is the Jacobian of the coordinate system.

In accordance with the choice of the toroidal angle ϕ,

$$g_{33} = R^2, \quad g^{33} = 1/R^2, \tag{B6}$$

where R is the radial coordinate in the cylindrical coordinate system (R,Z,ϕ), and g_{33} and g^{33} are the corresponding components of the metric tensor g_{ik} of the coordinate system (s,ϑ,ϕ) and of the inverse metric tensor g^{ik}. According to Eqs. (B4)–(B6)

$$B_0^3 = g^{33}B_{03} = F/R^2. \tag{B7}$$

Using Eqs. (B3), (B5), and (B7), we find the expressions for J and B_0^2:

$$J = fqR^2/F, \tag{B8}$$

$$B_0^2 = F/qR^2. \tag{B9}$$

The radial dependence of the function F is determined by the Grad–Shafranov equation averaged over the poloidal oscillations of the equilibrium magnetic field. This equation can be found in Refs. 7 and 9.

APPENDIX C: DERIVATION OF CURRENT CONTINUITY EQUATION

We express the pressure, number density, velocity, and the current of electrons and thermal ions as sums of their equilibrium and perturbed quantities (denoting the equilibrium parts by the subscript zero and the perturbations by tilde): $p_\alpha = p_{0\alpha} + \tilde{p}_\alpha$, $n_\alpha = n_{0\alpha} + \tilde{n}_\alpha$, $\mathbf{V}_\alpha = \mathbf{V}_{0\alpha} + \tilde{\mathbf{V}}_\alpha$; $\mathbf{j}_\alpha = \mathbf{j}_{0\alpha} + \tilde{\mathbf{j}}_\alpha$ $(\alpha = e,i)$, and introduce similar notations for the magnetic and electric field, $\mathbf{B} = \mathbf{B}_0 + \tilde{\mathbf{B}}$ and $\mathbf{E} = \tilde{\mathbf{E}}$. The perturbed densities of core ions and electrons are described by the continuity equations:

$$\partial\tilde{n}_\alpha/\partial t + \nabla\cdot(\tilde{n}_\alpha \mathbf{V}_{0\alpha} + n_{0\alpha}\tilde{\mathbf{V}}_\alpha) = 0, \tag{C1}$$

where $\alpha = (e,i)$.

It is assumed that the orbit width of the hot ions is infinitely large and that the orbit time is much shorter than the perturbation time scale (see in detail Ref. 6). Under these assumptions, the electric field of the perturbation acting on a hot ion is averaged along the large orbit of the hot ion and is negligibly small, $\langle\tilde{\mathbf{E}}\rangle \to 0$. Thus, the hot ions are not involved in the perturbed motion, and the quasineutrality condition for the perturbations takes the form [cf. Eq. (A8)]:

$$e_e\tilde{n}_e + e_i\tilde{n}_i = 0. \tag{C2}$$

Similarly, the total perturbed electric current $\tilde{\mathbf{j}}$ is given by

$$\tilde{\mathbf{j}} = \sum_{\alpha=e,i} \mathbf{j}_\alpha, \tag{C3}$$

where

$$\tilde{\mathbf{j}}_\alpha = e_\alpha(\tilde{n}_\alpha \mathbf{V}_{0\alpha} + n_{0\alpha}\tilde{\mathbf{V}}_\alpha). \tag{C4}$$

By combining the continuity equations (C1) for electrons and for the core ions, one obtains

$$\nabla_\parallel \tilde{j}_\parallel + \nabla_\perp\cdot(\tilde{\mathbf{j}}_{\perp e} + \tilde{\mathbf{j}}_{\perp i}) = 0, \tag{C5}$$

where $\tilde{\mathbf{j}}_{\perp e}$ and $\tilde{\mathbf{j}}_{\perp i}$ are the perpendicular (with respect to $\mathbf{B}_0$) perturbed electric currents of electrons and core ions and $\tilde{j}_\parallel$ is the parallel perturbed electric current.

In order to find the contribution of $\tilde{\mathbf{j}}_{\perp e}$ in Eq. (C5), we use the equation for the electron motion,

$$0 = -\nabla p_e + e_e n_e\left(\mathbf{E} + \frac{1}{c}[\mathbf{V}_e \times \mathbf{B}]\right), \tag{C6}$$

from which we obtain by linearizing and by neglecting the magnetic field curvature

$$\nabla_\perp\tilde{\mathbf{j}}_{\perp e} = e_e\tilde{\mathbf{V}}_E\cdot\nabla n_{0e} - \frac{c\mathbf{b}_0}{\mathbf{B}_0^2}([\nabla\tilde{p}_e\times\nabla B_0] + [\nabla p_{0e}\times\nabla\tilde{B}_\parallel]), \tag{C7}$$

where $\mathbf{b}_0 \equiv \mathbf{B}_0/B_0$, $\tilde{B}_\parallel = \mathbf{b}_0\cdot\tilde{\mathbf{B}}$, and

$$\mathbf{V}_E = c[\tilde{\mathbf{E}}\times\mathbf{B}_0]/\mathbf{B}_0^2 \tag{C8}$$

is the cross-field velocity due to the MHD perturbation with a perturbed electric field $\tilde{\mathbf{E}}$.

In order to find the contribution of $\tilde{\mathbf{j}}_{\perp i}$ into Eq. (C5), we use the equation for the core ion motion,

$$\rho\frac{d\mathbf{V}_i}{dt}=-\nabla p_i+e_i n_i\left(\mathbf{E}+\frac{1}{c}[\mathbf{V}_i\times\mathbf{B}]\right)-\nabla\cdot\vec{\pi}_\Lambda, \tag{C9}$$

where $\vec{\pi}_\Lambda$ is the gyroviscosity tensor,[9] $d/dt=\partial/\partial t+\mathbf{V}_i\cdot\nabla$, and ρ is the plasma mass density. One obtains then

$$\nabla_\perp\tilde{\mathbf{j}}_{\perp i}=\nabla_\perp\cdot\tilde{\mathbf{j}}^I+e_i\tilde{\mathbf{V}}_E\cdot\nabla n_{0i}-\frac{c\mathbf{b}_0}{\mathbf{B}_0^2}([\nabla\tilde{p}_i\times\nabla B_0]+[\nabla p_{0i}\times\nabla\tilde{B}_\parallel]), \tag{C10}$$

where $\tilde{\mathbf{j}}^I$ is the inertial part of the perpendicular current with the gyroviscosity included.

Substituting Eqs. (C7) and (C10) into Eq. (C5), we obtain the current continuity equation given by Eq. (1), where

$$H_p=-\frac{c\mathbf{b}_0}{\mathbf{B}_0^2}([\nabla\tilde{p}_c\times\nabla B_0]+[\nabla p_{0c}\times\nabla\tilde{B}_\parallel]), \tag{C11}$$

$$H_n=\mathbf{V}_E\cdot\nabla(e_e n_{0e}+e_i n_{0i}), \tag{C12}$$

and $\tilde{p}_c$ is the perturbed pressure of core plasma given by

$$\tilde{p}_c=\tilde{p}_e+\tilde{p}_i. \tag{C13}$$

Since the hot ions do not take part in the perturbed motion, one has

$$\tilde{p}_c=\tilde{p}, \tag{C14}$$

where $\tilde{p}$ is the total perturbed plasma pressure. The perturbed plasma pressure is related to $\tilde{B}_\parallel$ through the perturbed pressure balance equation:

$$\nabla\left(\frac{\tilde{B}_\parallel B_0}{4\pi}+\tilde{p}_c\right)=0, \tag{C15}$$

so that

$$\tilde{B}_\parallel=-4\pi\tilde{p}_c/B_0. \tag{C16}$$

Using Eqs. (A7) and (C16), we reduce Eq. (C11) to Eq. (2) while Eqs. (A8) and (C12) give Eq. (3).

APPENDIX D: DERIVATION OF SINGLE-FLUID MOMENTUM EQUATION

We sum Eqs. (C6) and (C9) and obtain

$$\rho\frac{d\mathbf{V}_i}{dt}+\nabla\cdot\vec{\pi}_\Lambda=-\nabla(p_e+p_i)+\frac{1}{c}[(\mathbf{j}_e+\mathbf{j}_i)_c\times\mathbf{B}]+(e_e n_e+e_i n_i)\tilde{\mathbf{E}}. \tag{D1}$$

Using Eq. (C8) we express the perpendicular electric field $\tilde{\mathbf{E}}_\perp$ in terms of $\mathbf{V}_E$:

$$\tilde{\mathbf{E}}=-\frac{1}{c}[\tilde{\mathbf{V}}_E\times\mathbf{B}]. \tag{D2}$$

The time dependence of the perturbed values is taken in the form $\exp(\lambda t)$, so that $\lambda=-i\omega$.

In linear approximation, one has[9]

$$\rho\frac{d\mathbf{V}_i}{dt}+\nabla\cdot\vec{\pi}_\Lambda\to\lambda\rho_0\tilde{\mathbf{V}}_E+\frac{cm_i}{e_i\mathbf{B}_0^2}[\mathbf{B}_0\times\nabla(\mathbf{V}_E\cdot\nabla p_{0i})]. \tag{D3}$$

Besides, allowing for Eqs. (A8) and (D2), one has in the linear approximation

$$(e_i n_i+e_e n_e)\mathbf{E}\to\frac{e_h n_{0h}}{c}[\tilde{\mathbf{V}}_E\times\mathbf{B}_0]. \tag{D4}$$

Similarly, in accordance with the discussion in Appendix C,

$$[(\mathbf{j}_e+\mathbf{j}_i)\times\mathbf{B}]\to[\tilde{\mathbf{j}}\times\mathbf{B}_0]+[\mathbf{j}_{0c}\times\tilde{\mathbf{B}}]. \tag{D5}$$

Allowing for Eqs. (A2) and (A3), we express

$$[\mathbf{j}_{0c}\times\tilde{\mathbf{B}}]=[\mathbf{j}_0\times\tilde{\mathbf{B}}]-\frac{c}{B_0}\tilde{B}_\parallel\nabla_\perp p_{0h}, \tag{D6}$$

and use Eq. (C16) in order to reduce Eq. (D1) to

$$\lambda\rho_0\tilde{\mathbf{V}}_E=-\nabla\tilde{p}_c+\frac{1}{c}[\mathbf{j}_0\times\tilde{\mathbf{B}}]+\frac{1}{c}[\tilde{\mathbf{j}}\times\mathbf{B}_0]-\frac{cm_i}{e_i\mathbf{B}_0^2}[\mathbf{B}_0\times(\tilde{\mathbf{V}}_E\cdot\nabla p_{0i})]+\frac{4\pi\tilde{p}_c}{\mathbf{B}_0^2}\nabla p_{0h}+\frac{e_h}{c}n_h[\tilde{\mathbf{V}}\times\mathbf{B}_0]. \tag{D7}$$

Without the two last terms on the right-hand side, Eq. (D7) coincides with the single-fluid momentum equation of Ref. 8. On the other hand, applying the operator $\mathbf{b}_0\cdot\nabla$ to Eq. (D7) and neglecting the curvature effects, one arrives at Eq. (1) with H_p and H_n given by Eqs. (2) and (3). This shows that the single-fluid momentum equation (D7) allows for both the pressure-dependent and density-dependent effects.

APPENDIX E: SINGLE-FLUID DESCRIPTION OF PERTURBED QUANTITIES

We express the magnetic and electric fields of the MHD perturbations in terms of the perturbed vector-potential $\mathbf{A}$:

$$\tilde{\mathbf{B}}=\nabla\times\mathbf{A}, \tag{E1}$$

$$\tilde{\mathbf{E}}=-\lambda\mathbf{A}/c, \tag{E2}$$

which is characterized by the covariant components A_1, A_2, and A_3. The perturbed fluid velocity vector $\mathbf{V}$ is characterized by the contravariant components V^1, V^2, and V^3. Introducing "optimized" variables similar to Ref. 7, i.e.,

$$\hat{A}_2\equiv[\mathbf{A}\times\mathbf{B}_0]^1/\mathbf{B}_0^2,\quad \hat{A}_3\equiv\mathbf{A}\cdot\mathbf{B}_0\equiv A_\parallel/B_0, \tag{E3}$$

$$\hat{V}^2\equiv[\mathbf{V}\times\mathbf{B}_0]_1,\quad \hat{V}^3\equiv\mathbf{V}\cdot\mathbf{B}_0/\mathbf{B}_0^2\equiv V_\parallel/B_0, \tag{E4}$$

we relate the perturbed magnetic field components $\tilde{B}^1$, $\tilde{B}^2$, and $\tilde{B}^3$ to A_1, $\hat{A}_2$, and $\hat{A}_3$ by (cf. Ref. 7)

$$\tilde{B}^1=\frac{1}{J}\left[\frac{\partial A_3}{\partial\vartheta}-\frac{\partial A_2}{\partial\phi}\right]$$
$$=\frac{1}{J}\left[-f\left(\frac{\partial}{\partial\vartheta}+q\frac{\partial}{\partial\phi}\right)\hat{A}_2 +F\left(\frac{\partial}{\partial\vartheta}-\frac{g_{22}}{qR^2}\frac{\partial}{\partial\phi}\right)\hat{A}_3\right], \quad \text{(E5)}$$

$$\tilde{B}^2=\frac{1}{J}\left[\frac{\partial A_1}{\partial\phi}+\frac{\partial}{\partial s}(f\hat{A}_2)\right], \quad \text{(E6)}$$

$$\tilde{B}^3=\frac{1}{J}\left[\frac{\partial}{\partial s}(fq\hat{A}_2)-\frac{\partial A_1}{\partial\vartheta}\right], \quad \text{(E7)}$$

while the perturbed velocity components are

$$\tilde{V}^2=\frac{F^2}{qR^2\mathbf{B}_0^2}\left(\frac{\hat{V}^2}{f}-\frac{g_{12}}{qR^2}\tilde{V}^1\right)+\frac{F\hat{V}^3}{qR^2}, \quad \text{(E8)}$$

$$\tilde{V}^3=-\frac{F^2}{qR^4\mathbf{B}_0^2}\left(\frac{g_{22}}{fq}\hat{V}^2+g_{12}\tilde{V}^1\right)+\frac{F\hat{V}^3}{R^2}. \quad \text{(E9)}$$

We obtain from Eqs. (D2) and (E2) the first two equations of our model, Eqs. (20) and (21). In order to obtain the two remaining equations of our model, we use the Maxwell equation

$$\nabla\times\tilde{\mathbf{B}}=4\pi\tilde{\mathbf{j}}/c, \quad \text{(E10)}$$

and represent the linearized equation of perturbed motion (D7) in the form:

$$\lambda\rho_0\left\{\tilde{\mathbf{V}}_E+\frac{c}{\mathbf{B}_0^2}\mathbf{B}_0\times\nabla\left(\frac{\hat{A}_2p_{0i}'}{n_0}\right)\right\}$$
$$=-\nabla\tilde{p}_c+\frac{\mathbf{H}}{4\pi}+\frac{e_h}{c}n_h[\tilde{\mathbf{V}}\times\mathbf{B}_0]+\frac{4\pi\tilde{p}_c}{B_0^2}\nabla p_{0h}, \quad \text{(E11)}$$

where

$$\mathbf{H}=(\nabla\times\mathbf{B}_0)\times\tilde{\mathbf{B}}-\mathbf{B}_0\times(\nabla\times\tilde{\mathbf{B}}). \quad \text{(E12)}$$

We only consider projections of Eq. (E11) perpendicular to the equilibrium magnetic field, which are important for our problem. These s, ϑ-covariant projections of the resulting equation lead to Eqs. (22) and (23).

APPENDIX F: SOLUTIONS OF EQ. (84) AND THEIR MATCHING TO SOLUTION (80)

The even and odd solutions to Eq. (84) $\phi_\pm$ are

$$\phi_+\sim F\left(\frac{1}{4}-\frac{i\alpha}{2},\frac{1}{4}+\frac{i\alpha}{2};\frac{1}{2};-\frac{x^2}{S}\right), \quad \text{(F1)}$$

$$\phi_-\sim xF\left(\frac{3}{4}-\frac{i\alpha}{2},\frac{3}{4}+\frac{i\alpha}{2};\frac{3}{4};-\frac{x^2}{S}\right), \quad \text{(F2)}$$

where F is the hypergeometrical function. Matching the asymptotic of the solution (80) for $x\ll 1$ with the asymptotic of solutions (F1) and (F2) for $x\gg S^{1/2}$ leads to dispersion relations for the even and odd modes, respectively, of the form (see in detail Sec. 5.1 of Ref. 18)

$$\left(\frac{S}{4}\right)^{i\alpha}=1+2i\alpha\left[2\psi(1)-\psi\left(\frac{1}{4}\right)\right], \quad \text{(F3)}$$

$$\left(\frac{S}{4}\right)^{i\alpha}=1+2i\alpha\left[2\psi(1)-\psi\left(\frac{3}{4}\right)\right], \quad \text{(F4)}$$

where $\psi(t)=\Gamma'(t)/\Gamma(t)$ is the psi-function. It hence follows that the eigenvalues $S=S_\pm$ of the even and odd modes are given by [cf. Eqs. (5.36) and (5.37) of Ref. 20]

$$S_+=2^8\exp\left(-\frac{2\pi l}{\alpha}-2C+\pi\right), \quad \text{(F5)}$$

$$S_-=2^8\exp\left(-\frac{2\pi l}{\alpha}-2C-\pi\right), \quad \text{(F6)}$$

where $l=1, 2, 3,\ldots$.

[1] C. D. Challis, X. Litaudon, G. Tresset, Yu. F. Baranov, A. Becoulet, C. Giroud, N. C. Hawkes, D. F. Howell, E. Joffrin, P. J. Lomas, J. Mailloux, M. J. Mantsinen, B. C. Stratton, D. G. Ward, K.-D. Zastrow, and contributors to the EFDA-JET work programme, Plasma Phys. Controlled Fusion **44**, 1031 (2002).
[2] M. J. Mantsinen, S. E. Sharapov, B. Alper, A. Gondhalekar, and D. C. McDonald, Plasma Phys. Controlled Fusion **42**, 1291 (2000).
[3] S. E. Sharapov, B. Alper, H. L. Berk, D. N. Borba, B. N. Breizman, C. D. Challis, A. Fasoli, N. C. Hawkes, T. C. Hender, J. Mailloux, S. D. Pinches, D. Testa, and contributors to the EFDA-JET work programme, Phys. Plasmas **9**, 2027 (2002).
[4] S. E. Sharapov, D. Testa, B. Alper, D. N. Borba, A. Fasoli, N. C. Hawkes, R. F. Heeter, M. J. Mantsinen, and M. von Hellermann, Phys. Lett. A **289**, 127 (2001).
[5] H. Kimura, Y. Kusama, M. Saigusa, G. J. Kramer, K. Tobita, M. Nemoto, T. Kondoh, T. Nishitani, O. Da Costa, T. Ozeki, T. Oikawa, S. Moriyama, A. Morioka, G. Y. Fu, C. Z. Cheng, and V. I. Afanas'ev, Nucl. Fusion **38**, 1303 (1998).
[6] H. L. Berk, D. N. Borba, B. N. Breizman, S. D. Pinches, and S. E. Sharapov, Phys. Rev. Lett. **87**, 185002 (2001).
[7] A. B. Mikhailovskii, G. T. A. Huysmans, W. O. K. Kerner, and S. E. Sharapov, Plasma Phys. Rep. **23**, 844 (1997).
[8] G. T. A. Huysmans, S. E. Sharapov, A. B. Mikhailovskii, and W. Kerner, Phys. Plasmas **8**, 4292 (2001).
[9] A. B. Mikhailovskii, Plasma Phys. Controlled Fusion **40**, 1907 (1998).
[10] W. Kerner, J. P. Goedbloed, G. T. A. Huysmans, S. Poedts, and E. Schwartz, J. Comput. Phys. **142**, 271 (1998).
[11] S. T. Tsai and L. Chen, Phys. Fluids B **5**, 3284 (1993).
[12] L. Chen, Phys. Plasmas **1**, 1519 (1994).
[13] F. Zonca and L. Chen, Phys. Plasmas **3**, 323 (1996).
[14] S. V. Konovalov, A. B. Mikhailovskii, V. S. Tsypin, and S. E. Sharapov, Dokl. Phys. **47**, 488 (2002).
[15] R. K. Varma and P. K. Shukla, Phys. Lett. A **196**, 342 (1995).
[16] A. B. Mikhailovskii and V. S. Tsypin, Nucl. Fusion **5**, 240 (1965).
[17] A. B. Mikhailovskii, *Electromagnetic Instabilities in an Inhomogeneous Plasma* (IOP, Bristol, 1992).
[18] A. B. Mikhailovskii, *Instabilities in a Confined Plasma* (IOP, Bristol, 1998).
[19] J. W. Connor, R. J. Hastie, T. J. Martin, and M. F. Turner, *in "Heating in Toroidal Plasmas,"* Proceedings of the 3rd Joint Varenna-Grenoble International Symposium, 1982, edited by C. Gormezano, G. G. Leotta, and E. Sindoni (Commission of the European Communities, Euratom, Brussels, 1982), Vol. 1, p. 65.
[20] B. N. Breizman, H. L. Berk, M. S. Pekker, S. D. Pinches, and S. E. Sharapov, Phys. Plasmas **10**, 3649 (2003).
[21] M. N. Bussac, R. Pellat, D. Edery, and J. L. Soule, Phys. Rev. Lett. **35**, 1638 (1975).
[22] A. B. Mikhailovskii, *Theory of Plasma Instabilities* (Consultants Bureau, New York, 1974), Vol. 2.
[23] A. B. Mikhailovskii and A. A. Skovoroda, Plasma Phys. Controlled Fusion **44**, 2033 (2002).

[24]D. N. Borba, H. L. Berk, B. N. Breizman, A. Fasoli, F. Nabais, S. D. Pinches, S. E. Sharapov, D. Testa, and contributors to the EFDA-JET Work Programme, Nucl. Fusion **42**, 1029 (2002).
[25]R. Nazikian, G. J. Kramer, C. Z. Cheng, N. N. Gorelenkov, H. L. Berk, and S. E. Sharapov, Phys. Rev. Lett. **91**, 125003 (2003).
[26]A. Fukuyama and E. Yokota, ''Analysis of Alfvén eigenmode in toroidal plasmas with negative magnetic shear,'' Japan Atomic Energy Research Institute Rep. No. JAERI-Conf 2000-004 (2000), p. 61.
[27]S. Migliuolo, Nucl. Fusion **33**, 1721 (1993).
[28]N. N. Gorelenkov, M. J. Mantsinen, S. E. Sharapov, and C. Z. Cheng, in *Proceedings of the 30th European Conference on Controlled Fusion and Plasma Physics*, edited by R. Koch and S. Lebedev (European Physical Society, St. Petersburg, Russia, 2003), P-2.100.
[29]C. D. Challis, Yu. F. Baranov, G. D. Conway, C. Gormezano, C. W. Gowers, N. C. Hawkes, T. C. Hender, E. Joffrin, J. Mailloux, D. Mazon, S. Podda, R. Prentice, F. G. Rimini, S. E. Sharapov, A. C. C. Sips, B. C. Stratton, D. Testa, and K.-D. Zastrow, Plasma Phys. Controlled Fusion **43**, 861 (2001).